Theoretical Analysis of Core Size Effect in Metalloporphyrins[†]

Pawel M. Kozlowski,*,‡ Jason R. Bingham,§ and Andrzej A. Jarzecki*,§

Department of Chemistry, University of Louisville, Louisville, Kentucky 40292, and Department of Chemistry, Brooklyn College and the Graduate School of the City University of New York, Brooklyn, New York 11210

Density functional theory has been applied to a series of unsubstituted planar metalloporphyrins (MPs) to elucidate how geometry and frequencies correlate with the metal−nitrogen distance, referred to as the core size. Different transition metals can invoke expansion or contraction of the porphyrin core due to electronic effects resulting from the amount of d-electron pairing as well as occupancy of the $d_{x^2-y^2}$ orbital. A full vibrational analysis consisting of all in-plane and out-of-plane frequencies was carried out, and the resulting modes were plotted against core size for a linear analysis and grouped within symmetry blocks. The modes were separated according to planarity, and all modes with a large slope and best fit greater than 0.8 were considered sensitive to metal−nitrogen distances. All planar skeletal modes above 1450 cm^{-1}, including the pyrolle ring deformations, are found to be core-size sensitive. The most significant out-of-plane modes sensitive to core size are γ_8 and γ_9, which are infrared active and grouped within the A_{2u} symmetry block. The present work also opens possible quantitative applications for the correlation of spectroscopic properties of MPs and heme proteins with actual structural parameters.

1. Introduction

Metalloporphyrins (MPs; Figure 1), most often found in the active site of proteins, continue to be the subject of active research, particularly in the studies of heme proteins and photoreaction centers.[1] Various experimental techniques have been applied to study MP complexes, both as isolated systems and as active sites within the protein environment. One of the most useful techniques used for probing MP complexes is vibrational spectroscopy, specifically resonance Raman (RR),[2] which utilizes laser excitation of the $\pi \rightarrow \pi^*$ absorption maximum.[3] Hence, enhancement of totally symmetric, in-plane modes is typically expected upon this excitation.

Direct correlation of vibrational spectra with structure is generally difficult and has always been recognized as a limitation of vibrational spectroscopy. However, by early recognition of structure-sensitive marker bands associated with oxidation and spin states of MPs,[4] vibrational spectra have provided a unique perspective for the application of RR spectroscopy. The capability of probing vibrations in the porphyrin macrocycle—that can be directly correlated with structure—reflects the fact that the macrocycle has a planar, π-conjugated structure with D_{4h} symmetry (Figure 1). The macrocycle cavity can accommodate a variety of transition metals and, in the cases such as iron-containing porphyrins, multiple oxidation states. These differences in metal or oxidation state result in measurable changes in distance between the center metal atom and the pyrrole nitrogen atom (M−N), referred to as the core size.

The effects of different metals and peripheral substituents on porphyrin core size have been probed with X-ray crystal-lography, beginning with studies conducted by Hoard in the early 1970s.[5] Using X-ray data from several Ni, Zn, Sn, Fe, and Mg substituent porphyrin systems, Hoard deduced that metals play a key role in core changes that render the rigidity of the macrocycle system. On the other hand, vibrational markers have long been sought as quantitative indicators of structural changes in the porphyrin systems, ever since it was recognized that shifts in RR spectra can correlate to structural changes in metal oxidation and spin states.[4,6] Spaulding et al.[7] discovered that the frequency of an anomalously polarized ν_{19} band, assigned as C_α−N asymmetric stretching, correlates negatively with the porphyrin core size in a series of structurally determined metallo-octaethylporphyrins (MOEP). A subsequent analysis by Choi et al.[8] concluded that all skeletal modes above 1450 cm^{-1} for the studied Fe- and Ni-substituted metallo-protoporphyrin (MPP) structures have a negative linear correlation with core size, which was attributed to the dependence of the force constant for methine bridge bonds. Parthasarathi et al.[9] re-examined the RR frequencies for a wider range of MPP and metallo-tetraphenylporphyrin (MTPP) systems and generalized trends in skeletal modes. They also went beyond the normally studied Ni and Fe porphyrins to investigate general trends for Sn, Mn, and Co PP and TPP complexes, including deviations due to spin state and oxidation. Interestingly, they found that linear correlations seem to break down for Sn^{IV} complexes due to "saturation of the core size effect" as a result of the large core that Sn^{IV} imposes.

The most comprehensive analysis of core size expansion and nonplanarity effects on MP vibrational frequencies has been reported by Prendergast and Spiro.[10] A wide variety of substituted porphyrins have been examined by employing crystallographic data and empirical force fields to establish the relationship between the skeletal modes and the core size. Semiempirical QCFF/Pi and MNDO/3 calculations were carried out to quantify observed correlations. Special emphasis was placed on the ν_{10} and ν_{19} modes, which have often been used to describe the ruffling or doming kinematics of porphyrins.

* To whom correspondence should be addressed. (P.M.K.) Tel: +1-502-852-6609. Fax: +1-502-852-8149. E-mail: pawel@louisville.edu. (A.A.J.) Tel: +1-718-951-5000ext. 2822. Fax: +1-718-951-4607. E-mail: jarzecki@brooklyn.cuny.edu.
‡ University of Louisville.
§ Brooklyn College and the Graduate School of the City University of New York.

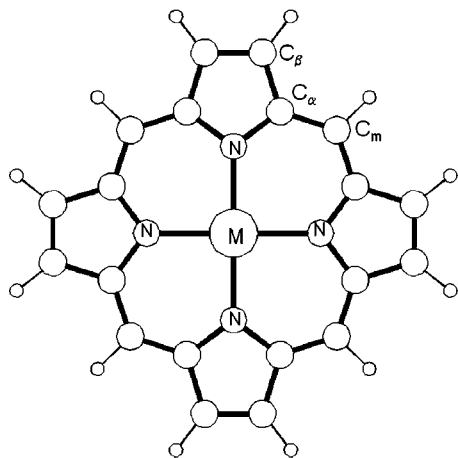**12782** *J. Phys. Chem. A, Vol. 112, No. 50, 2008*

Kozlowski et al.

Figure 1. Structure and atom labeling scheme for MPs.

The structural changes associated with $C_\alpha-C_m$, $C_\alpha-C_\beta$, and $C_\beta-C_\beta$ bonds, $C_\alpha C_m C_\alpha$ angles, and contraction of $C_\alpha-N$ distance were also investigated in conjunction with core size for a wide range of octaethylporphyrin (OEP) and tetraphenylporphyrin (TPP) metal complexes.

While the "core size effect" has been known for some time, there is no record of "first principles" methods of computational chemistry having been applied to quantify it. There has been no attempt to perform a full vibrational analysis over a range of MP complexes with a variety of d-metals in an attempt to elucidate the link between structure and frequency. The experimental data, on which the core size hypothesis has been relayed (refs 7–9), need to be complemented by computational study for two reasons: (i) Only a limited set of frequencies can be obtained from experiment, that is, primarily in-plane, RR active modes, and (ii) vibrational data available for MPs are typically influenced by peripheral substituents and effects associated with nonplanarity. This study is designed to present density functional theory (DFT) calculations for series of MPs in an effort to examine all of the vibrational differences due to changes within the macrocycle core. In that respect, all major bond lengths and angles, as well as related vibrational frequencies, have been calculated and analyzed for MPs (Figure 1) with a series of first row (d^4-d^{10}) transition metals.

2. Computational Details

Reported calculations were carried out using nonlocal density DFT with Becke−Lee−Yang−Parr (B3LYP) functional and 6-31G(d) basis set employing the Gaussian 03[11] suite of programs for electronic structure calculations. This level of theory has proven appropriate for structure and vibrational analysis of MPs with excellent agreement of experimental data in previous studies.[12–16] To establish correlation between the structure and the vibrational properties, unsubstituted planar porphines were utilized, incorporating a series of first row (d^4-d^{10}) transition metals in the center. The geometry of each MP was optimized, and a full vibrational analysis was carried out assuming D_{4h} symmetry constraints. The ground-state electronic configuration was verified by testing of the stability of the wave function. In all cases, it was verified that the optimized structures correspond to the stable minima with an exception for Ni-porphine, for which one imaginary frequency was found. This imaginary frequency is associated with the ruffling of the porphine macrocycle as has been demonstrated previously.[13] To improve the quality of the vibrational force field, a set of nonredundant internal coordinates was generated

and Cartesian force constants were transferred to internal force constants.[17] The internal force constants were scaled according to a scaled quantum mechanical (SQM) procedure.[18] Following our previous studies, we applied six scaling factors, which have been thoroughly investigated for other MPs.[13–15] In addition, we have obtained the total energy distribution (TED) of each vibrational mode in terms of stretches, bends, torsions, etc.

3. Results and Discussion

3.1. Geometric Parameters−Dependence on Core Size. MPs are planar, conjugated systems with D_{4h} symmetry capable of accommodating various metals. The system is sensitive to small changes in the M−N bond length, and the experimentally measured variation in the M−N length ranges from 1.93 to 2.10 Å, typically observed in MOEP[7,10] and MTPP.[10] For relatively small values of core size, the porphyrin ring undergoes out-of-plane distortion (ruffling), which is typically observed for complexes with nickel.[13] However, in the case of large core sizes, such as those with Mn[10] or Mo,[19] doming is a preferable distortion of the porphyrin macrocycle. To cover the range of experimentally observed M−N bond lengths, seven first-row MP complexes with increasing number of d-electrons (d^4-d^{10}) have been analyzed with respect to the most important geometric parameters extracted from DFT calculations. Those structural parameters, including unique bond lengths and bond angles, are collected in Tables 1 and 2.

Core size dependence plotted as a function of the number of d-electrons (Figure 2) reveals that the largest core size (2.087 Å) is observed for MnP, while the smallest (1.960 Å) is observed for NiP. The dependence of core size as a function of number of d-electrons can be readily explained in terms of occupancy of metal d-orbitals. The larger core size observed for MnP is a consequence of the high spin d^5 sextet state, in which each d-orbital is singly occupied, including the highest energy $d_{x^2-y^2}$ orbital. The smaller core size measured for NiP is attributed to d^8 singlet configuration, in which eight electrons doubly occupy manifold of d-orbitals leaving the $d_{x^2-y^2}$ empty. Consequently, the addition (d^9 Cu) or removal (d^7 Co) of an electron from NiP d-orbitals results in an increase of the core size. The removal of an electron (d^7 Co configuration) results in a low spin (doublet) configuration with the M−N distance falling between values found for the singlet d^8 Ni and triplet d^6 Fe configurations. Introducing a second electron to the $d_{x^2-y^2}$ orbital leads to fully occupied d-orbitals (d^{10} Zn), resulting in the expected increase of the M−N distance.

Conversely, the addition or removal of an electron from high spin (d^5 Mn configuration) decreases the core size due to the absence of an electron in the $d_{x^2-y^2}$ orbital. The quintet of the d^4 Cr configuration leads to the decreased core size (2.048 Å) that is similar to singlet d^{10} ZnP (2.046 Å). On the other hand, addition of an electron to the d^5 Mn configuration may produce several different low-lying electronic states of iron porphines. Different electronic states of FeP were analyzed in previous studies,[12] and some of them have been included for comparison in Tables 1 and 2. As expected, because of $d_{x^2-y^2}$ orbital electron population, the core size for triplet ($^3A_{2g}$ and $^3B_{2g}$) FeP states ($\sim$2.00 Å) is smaller than that found for the high spin quintet ($^5A_{1g}$ and $^5B_{2g}$) FeP configurations ($\sim$2.06 Å).

In an effort to explain the changes associated with the core size effect, the bond lengths $C_\alpha-C_\beta$, $C_\alpha-C_m$, $C_\beta-C_\beta$, and N−C_α (Figure 3a) and angles $C_\alpha C_m C_\alpha$, N$C_\alpha C_m$, $C_\alpha C_\beta C_\beta$, $C_\beta C_\alpha C_m$, N$C_\alpha C_\beta$, $C_\alpha NC_\alpha$, and MNC_α (Figure 3b,c) were plotted as a function of M−N. With increasing core size, the rigid porphine skeleton compensates by adjusting other geometric

Analysis of Core Size Effect in Metalloporphyrins

J. Phys. Chem. A, Vol. 112, No. 50, 2008 **12783**

TABLE 1: Selected Bond Lengths (Å) of Calculated MPs and Slopes of Associated Core-Size Correlation Plots

| | Cr | Mn | Fe[a] | | | | | Co | Ni | Cu | Zn | slopes |
			$^3A_{2g}$	$^5A_{1g}$	$^3B_{2g}$	$^5B_{2g}$	$^1A_{1g}$					
$M-N_p$	2.042	2.083	2.001	2.061	1.993	2.061	2.002	1.976	1.957	2.007	2.046	
$N-C_\alpha$	1.377	1.372	1.377	1.373	1.379	1.372	1.377	1.381	1.381	1.376	1.372	−0.078
$C_\alpha-C_m$	1.395	1.404	1.388	1.400	1.387	1.400	1.388	1.383	1.380	1.388	1.396	0.188
$C_\alpha-C_\beta$	1.444	1.448	1.441	1.446	1.440	1.447	1.442	1.440	1.439	1.443	1.446	0.074
$C_\beta-C_\beta$	1.364	1.366	1.362	1.365	1.361	1.366	1.360	1.359	1.358	1.361	1.363	0.063

[a] Both high and low spin data are reported here; however, only the triplet $^3B_{2g}$ was employed in the core-size analysis.

TABLE 2: Selected Bond Angles (Degrees) of Calculated MPs and Slopes of Associated Core-Size Correlation Plots

| | Cr | Mn | Fe[a] | | | | | Co | Ni | Cu | Zn | slopes |
			$^3A_{2g}$	$^5A_{1g}$	$^3B_{2g}$	$^5B_{2g}$	$^1A_{1g}$					
$M-N-C_\alpha$	126.7	126.1	127.3	126.4	127.5	126.4	127.3	127.7	128.0	127.2	126.6	−14.981
$C_\alpha-N-C_\alpha$	106.6	107.8	105.1	107.2	105.1	107.1	105.4	104.5	104.1	105.6	106.7	29.973
$N-C_\alpha-C_m$	125.1	125.0	125.7	125.1	125.2	125.0	125.2	125.2	125.3	125.2	125.1	−2.501
$N-C_\alpha-C_\beta$	109.7	109.0	110.6	109.4	110.7	109.5	110.6	111.1	111.4	110.5	109.8	−19.176
$C_\beta-C_\alpha-C_m$	125.2	126.0	124.2	125.5	124.0	125.6	124.2	123.7	123.3	124.3	125.1	21.668
$C_\alpha-C_m-C_\alpha$	126.4	127.9	124.9	127.0	124.6	127.0	125.1	124.2	123.4	125.2	126.5	34.964
$C_\alpha-C_\beta-C_\beta$	107.0	107.1	106.7	107.0	106.7	106.9	106.7	106.6	106.6	106.7	106.9	4.186

[a] Both high and low spin data are reported here; however, only the triplet $^3B_{2g}$ was employed in the core-size analysis.
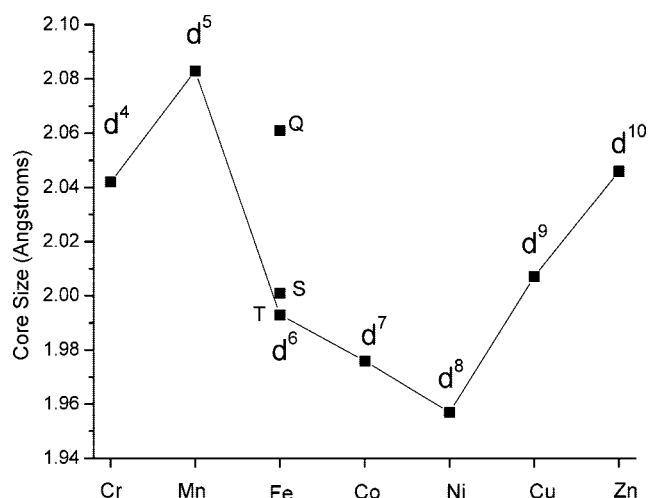

Figure 2. Diagram of core size (Å) as a function of 3d-orbital occupation for various transition metals. In the case of FeP (d⁶), the core sizes of the (S) singlet, (T) triplet, and (Q) quintet spin states are shown.

parameters. For bond lengths, a positive linear correlation for $C_\alpha-C_\beta$, $C_\alpha-C_m$, and $C_\beta-C_\beta$ and a negative linear correlation for $N-C_\alpha$ is observed, analogous to trends observed in crystallographic data and QCFF/Pi semiempirical calculations by Spiro and co-workers.[10] However, their results for $C_\beta-C_\beta$ bond distances did not follow experimental trends. DFT calculations were able to provide results with better agreement to experimental data especially for the $C_\beta-C_\beta$ distance, which may reflect the fact that unsubstituted porphines were used in the present analysis. The macro-ring of the porphyrins with $C_\alpha-C_\beta$, $C_\alpha-C_m$, and $C_\beta-C_\beta$ distances increases linearly with core size. The quality of all fitted data was judged by least-squares R^2 values. With exemption of the $N-C_\alpha$ plot ($R^2 = 0.79$), all macro-ring stretches have good correlation with linearity as shown in Table 1. It is assumed that the $N-C_\alpha$ bond acts as a spring, compensating for the outward expansion of the other bonds.

Negative slopes are only found for angles containing the $N-C_\alpha$ bond, further supporting the hypothesis that this parameter compensates for the outward strain placed on the rigid

system when increasing the M—N distance. The correlation of angles (Figures 3b,c) to the core size is more complicated and best explained by trends observed for a pyrrole ring and a methane bridge. An interesting hypothesis to the characterization of pyrrole ring changes was presented by Warshel,[20] in which he proposed that pyrrole rings in porphyrin systems behave as rigid units. It was suggested that the strain induced by expansion of the core is relieved by lengthening of the $C_\alpha-C_m-C_\alpha$ bonds, the so-called methine bridges. Using the calculated DFT data, we tested this hypothesis by superimposing two pyrrole rings: first NiP with the shortest M—N bond length and the second MnP with the longest M—N bond. This geometry comparison indeed supports Warshel's contention. The pyrrole rings do not significantly change shape; however, a slight elongation of the $C_\beta-C_\alpha$ bond is observed that scales linearly with core size. Also, the $C_\beta-C_\beta$ bond remains unaffected, and the most sensitive bond lengths are the $C_\alpha-C_m$ arms and the $C_\alpha-N-C_\alpha$ bond angles. Therefore, in a first approximation, it may be assumed that the rings are not affected by the core expansion. The same effect was noted empirically by Sparks et al.[21] for substituted porphyrins. Consequently, only the $C_\alpha-C_m-C_\alpha$ angles and associated vibrations, as is presented in the next section, are the most sensitive for core size expansion.

3.2. Vibrational Frequencies. To establish a correlation between core size and structure-sensitive modes for the unsubstituted MP complexes, a vibrational analysis was performed employing SQM refinement of DFT force fields as briefly described in the computational section. Utilizing a highly symmetrical, planar structure of analyzed MPs, all 105 vibrations were separated to in-plane (ip) and out-of-plane (oop) vibrations as $\Gamma_{tot} = 71\Gamma_{ip} + 34\Gamma_{oop}$ and further categorized into symmetry blocks. According to D_{4h} symmetry, $71\Gamma_{ip} = 9A_{1g} + 9B_{1g} + 8A_{1g} + 9B_{2g} + 18E_u$ and $34\Gamma_{oop} = 3A_{1u} + 5B_{1u} + 6A_{2u} + 4B_{2u} + 8E_g$. Although the true energy minimum for Ni-porphine is ruffled[13] (structure has D_{2d} symmetry), for consistency of the analysis, a planar D_{4h} symmetry structure with one imaginary frequency (γ_{14}) was employed for the NiP complex. Labeling the MP modes follows a conventional notation;[6,22] in-planes are labeled as ν_{1-53}, and out-of-plane modes are labeled as γ_{1-26} (note that all doubly degenerate E modes are labeled once). In addition, following earlier work of Spiro and co-workers,[22] the

12784 *J. Phys. Chem. A, Vol. 112, No. 50, 2008*

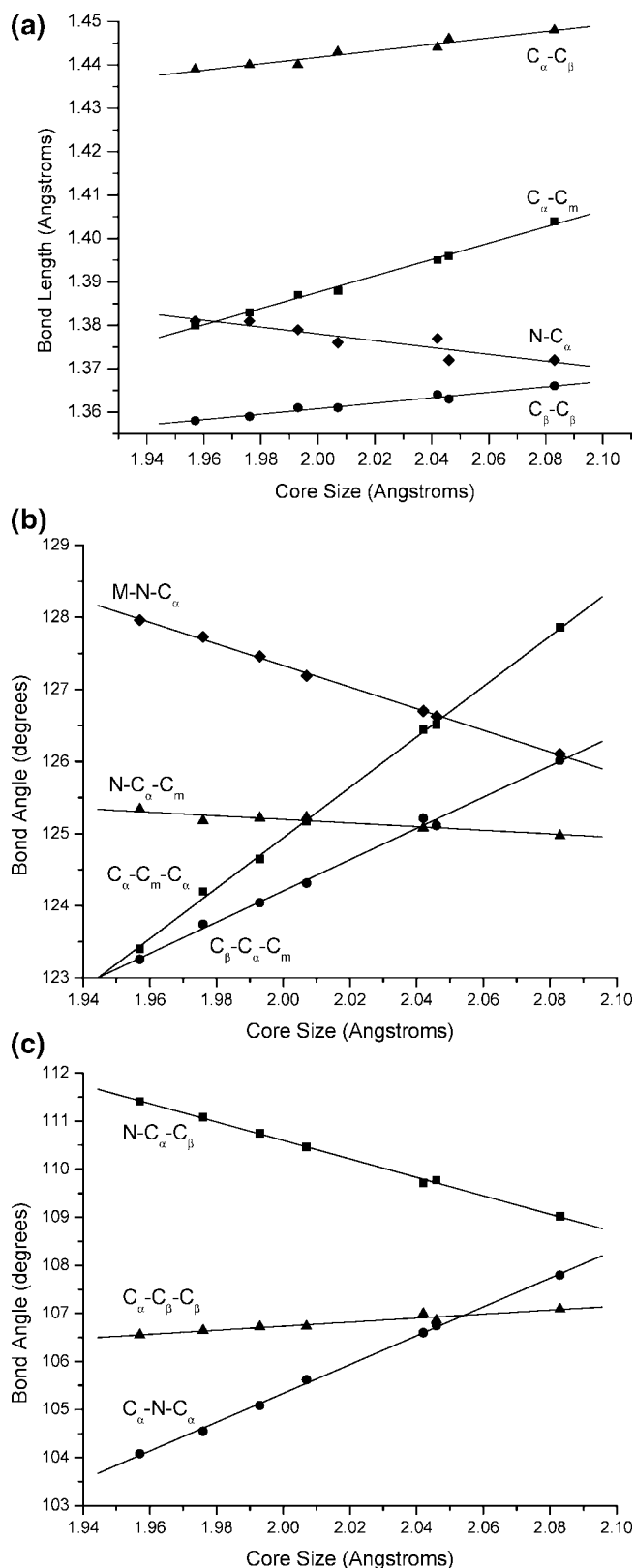Kozlowski et al.

(a)

(b)

(c)

Figure 3. Correlation plots of selected bond distances (Å) vs the core size (Å) for the MPs (a). Correlation plots of selected bond angles (degrees) vs core size (Å) for the MPs (b and c).

local coordinate framework was used to describe modes and assign computed fundamentals. All ip and oop frequencies and mode assignments are shown in the Supporting Information (Tables S1 and S2), in which the vibrations are grouped according to symmetry and arranged as a function of core size.
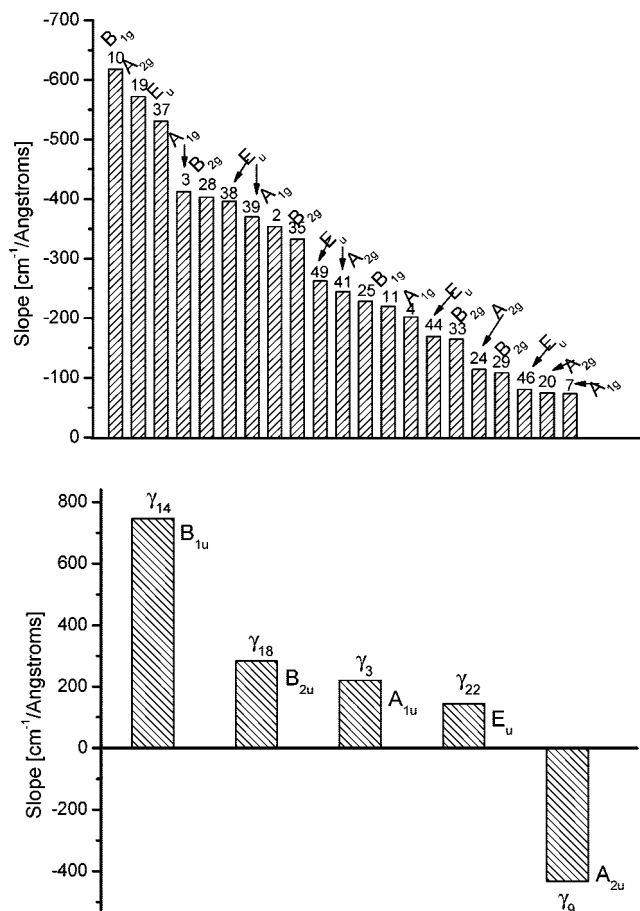

Figure 4. Histogram of calculated frequency slopes (cm^{-1}/Å) for (top) in-plane and (bottom) out-of-plane fundamentals of MPs. Labels identify the symmetry and the assignment of selected normal modes.

Further characterization of these vibrations is presented in graphical form as functions of increasing core size and their best least-squares fit lines (Supporting Information, Figures S-in-planes). The quality of the fit was judged by the R^2 value, which is listed for each frequency set in Tables S1 and S2 of the Supporting Information, along with the slope and the intercept of the line. Almost all of the analyzed frequencies correlate linearly with the core size. Only a small subset, mainly oop modes, has rather low R^2 values. Frequency modes, with a strong linear correlation ($R^2 > 0.86$), have significant sensitivity (large slope value) with respect to core size. These frequencies cover the most important range of core sensitive modes. They are marked in Tables S1 and S2 of the Supporting Information by the bold face and are subject of further total energy distribution (TED) analysis (see below).

The frequency–slope correlation is summarized in Figure 4 (top) for ip modes and (bottom) for oop modes. Presentation of these modes excludes all C–H stretch and C–H out-of-plane modes, which are not relevant for substituted MPs. The overall correlation for ip modes shows that the majority of vibrations decrease as the size of the core increases (Figure 5). The most notable modes that have largest slopes (Figure 5, left) with respect to core size (ν_2, ν_3, ν_{10}, ν_{19}, ν_{28}, ν_{37}, ν_{38}, and ν_{39}) are all the planar skeletal modes above 1450 cm^{-1}. Computational prediction of these modes is in agreement with experimentally determined core sensitive modes previously reported in literature.[7–10] It has been noted in the literature that the skeletal modes with higher frequencies tend to have vibrations involving the C_α–C_m stretch, and lower frequencies (those closer to 1450 cm^{-1}) have a more C_β–C_β stretching character.[10] These

Analysis of Core Size Effect in Metalloporphyrins
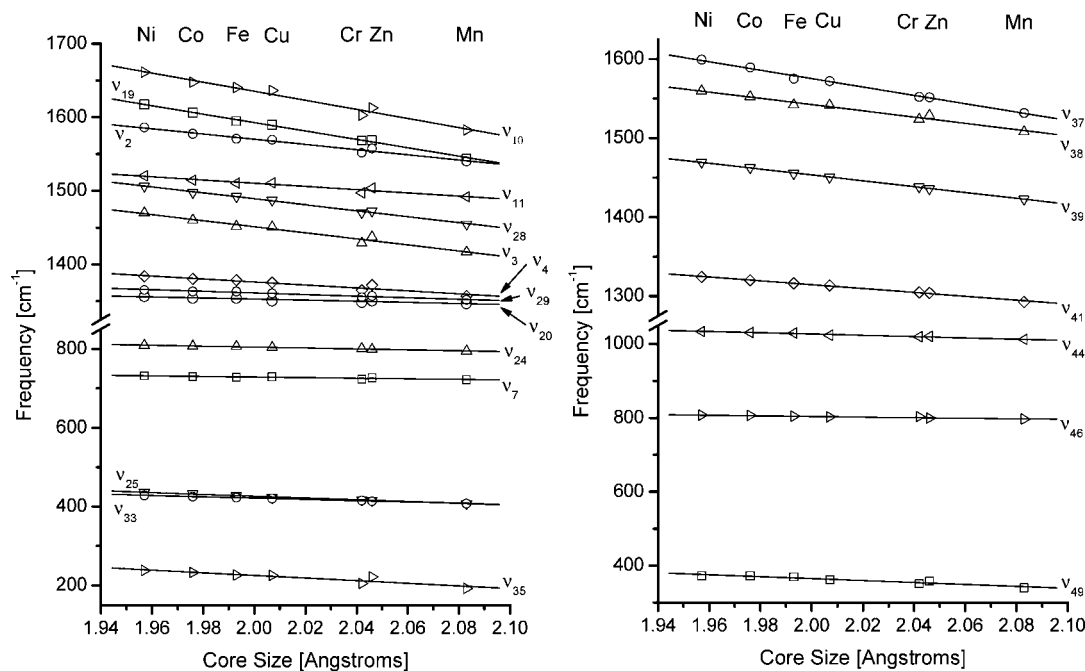
J. Phys. Chem. A, Vol. 112, No. 50, 2008 **12785**

Figure 5. Correlation plots of selected in-plane frequencies (cm^{-1}) vs core size (Å) for MPs. Left panel, frequencies of the A_{1g}, A_{2g}, B_{1g}, and B_{2g} symmetries. Right panel, frequencies of the E_u symmetry.

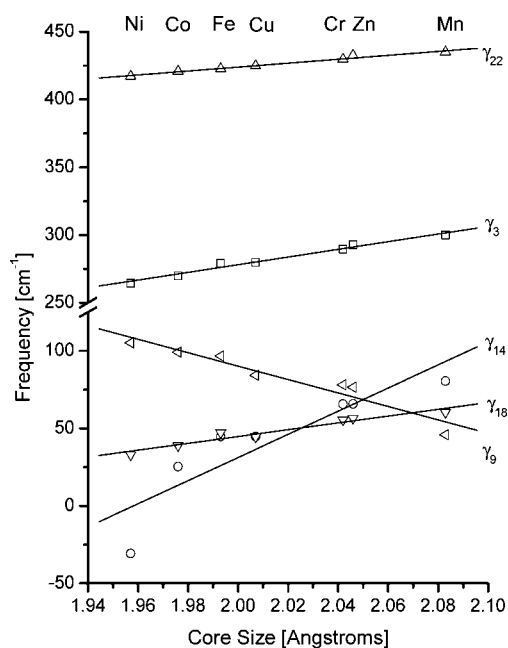**Figure 6.** Correlation plots of selected out-of-plane frequencies (cm^{-1}) vs core size (Å) for MPs.

two stretches C_α–C_m and C_β–C_β give the largest variation with respect to core size, as indicated by their slopes in Table 1 and Figure 3. The first four ip modes with the largest slopes (ν_{10}, ν_{19}, ν_{37}, and ν_3 shown in Figure 5) are all out-of-phase C_α–C_m stretches. Similarly, in-phase C_α–C_m stretches (ν_{28} and ν_{39}) are also very sensitive to core changes. The C_α–C_m bond lengths have long been recognized[7] to significantly differ with metal core size for various substituted porphyrin systems due to their involvement in the conjugated outer periphery that compensates for core changes. Modes ν_{38}, ν_2, and ν_{11} contain noticeable contribution of C_β–C_β stretches, which are saturated periphery bonds sensitive to the core. Some planar modes are considered nonskeletal because the majority of their vibrations are located around the center pyrole nitrogens instead of the outer periphery

bonds. These modes can also show a sensitivity to core metal occupancy. The most notable nonskeletal modes are ν_{35}, ν_{49}, ν_{41}, ν_{25}, and ν_4, listed in order of decreasing linearity.

In the case of oop modes, the most significant, nonhydrogen modes with the largest slope values are γ_3 (A_{1u}), γ_9 (A_{2u}), γ_{14} (B_{1u}), γ_{18} (B_{2u}), and γ_{22} (E_g), which correspond to propeller, doming, ruffling, saddling, and pyrole rings swivel distortions, respectively (Table S2 of the Supporting Information, Figure 4, bottom, and Figure 6). Other significant slope values computed for oop modes are found only for symmetric and asymmetric C_β–H modes, which are not relevant for commonly β-substituted porphyrins, and for γ_{16} (B_{2u} pyrole tilting). However, a linear correlation for this fundamental is a quite poor ($R^2 = 0.65$). As expected, a majority of the out-of-plane core-sensitive modes involve distortion of the M–N core (ruffling, doming, waving, etc.), which tend to have lower frequencies within the oop modes.

3.3. Total Energy Distribution. To establish how structure-sensitive modes depend on particular structural elements, each vibration has been analyzed with respect to total energy distribution (TED). The TED analysis describes essential contributions of elemental coordinates such as stretching, bending, or torsion in vibrational modes. In the analysis, we have applied the same set of nonredundant internal coordinates that was used to define the SQM force field. A convenient way to present this analysis is to list the results within symmetry blocks. In-plane symmetry modes, A_{1g}, A_{2g}, B_{1g}, and B_{2g}, are Raman-active and might be confirmed by RR data, while symmetry modes, E_u (ip) and A_{2u} (oop), are infrared-active and can be verified through IR data. Figure 7 exemplifies an analysis of TED data as plotted changes in percentage of internal coordinate contributions for selected vibrational modes ν_2, ν_4, ν_{10}, and ν_{19} that exhibit a noticeable dependence on core size. The full analysis of all modes can be found in the Supporting Information (Figure S-ip).

Among the vibrations of symmetry A_{1g}, B_{1g}, B_{2g}, and A_{2g} that can be detected via RR spectroscopy, the most important are the totally symmetric A_{1g} modes. These modes have been used
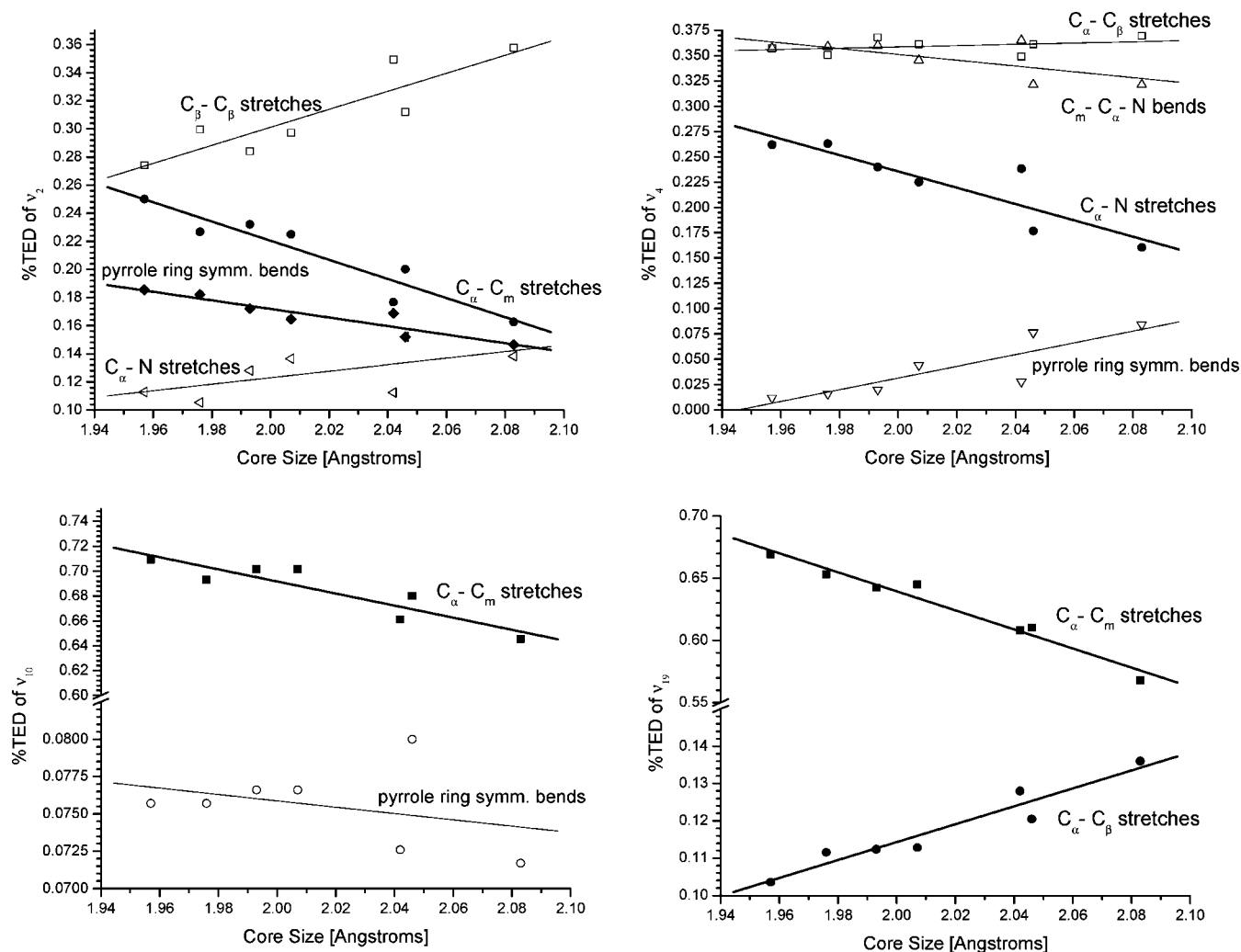
Figure 7. Correlation plots of %TED for ν_2, ν_4, ν_{10}, and ν_{19} in-plane frequencies (cm^{-1}) vs core size (Å). All TED values are normalized to 1.00 (i.e. %TED/100). Open symbols represent linear correlation with $R^2 < 0.90$, while closed with $R^2 > 0.90$, respectively.

as oxidation or spin state markers when enhanced by laser excitation of the Soret (or B) band. The sensitivity of these modes with respect to spin state or oxidation changes reflects changes in the core size associated with the M−N expansion or contraction. The individual breakdown in total energy distribution for modes within A_{1g} (ν_2, ν_3, ν_4, and ν_7) is shown in Figure 7 and S-ip (Supporting Information). Mode ν_2 is comprised of mostly C$_\beta$−C$_\beta$ (positive correlation) and C$_\alpha$−C$_m$ (negative correlation) stretching character as core size increases. There is also an approximate 2% increase in N−C$_\alpha$ stretching character over the core size range. Mode ν_3 has greater C$_\beta$−C$_\beta$ stretching character (negative correlation) and also some C$_\alpha$−C$_m$ stretching character, which oscillates between 26−30% over the core size range. The N−C$_\alpha$ stretching increases as a function of core size. Mode ν_4 has approximately 36% C$_\alpha$−C$_\beta$ stretching character, which is consistent for each metal, and a decrease in the N−C$_\alpha$−C$_m$ bond angle and N−C$_\alpha$ bond character.

The RR-active modes upon Q-band excitation of symmetry B_{1g}, A_{2g}, and B_{2g} are among the most sensitive with respect to core expansion. Two of these modes, ν_{10} (B_{1g}) and ν_{19} (A_{2g}), have the highest sensitivity with respect to M−N distances and slopes greater than −550 cm^{-1}/Å (Table S1 of the Supporting Information and Figure 4, top). The TED analysis reveals that both modes have significant contributions from C$_\alpha$−C$_m$ stretching of the methane bridges. Mode ν_{19} is a skeletal mode with mostly C$_\alpha$−C$_m$ character and a negative correlation to core size.

The ν_{11} mode of B$_{1\ g}$ shown in Figure S-ip of the Supporting Information has the kinetic energy localized mostly at C$_\beta$−C$_\beta$ stretching.

Symmetry block A_{2g} is comprised of skeletal modes ν_{19}, ν_{20}, ν_{24}, and ν_{25} (Figures 7 and S-ip of the Supporting Information). Mode ν_{19} is a strong planar skeletal mode with mostly C$_\alpha$−C$_m$ character and a negative correlation to core size. Mode ν_{20} has strongly core size-dependent kinetic energy distribution localized in C$_\alpha$−C$_\beta$ stretching. Mode ν_{24} has a minor contribution from C$_\alpha$−C$_\beta$ stretching but is mostly characterized by the asymmetric bending of the pyrrole rings resulting in a "wiggling" effect. The vibration of mode ν_{25} is almost completely characterized by bending of the N−C$_\alpha$−C$_m$ angle. All linear modes within this symmetry block are distinguished by changes along the periphery.

The core-sensitive modes within B_{2g} symmetry are ν_{28}, ν_{29}, ν_{33}, and ν_{35} (Figure S-ip of the Supporting Information). The skeletal mode ν_{28} has mostly C$_\alpha$−C$_m$ character (negative correlation). Modes ν_{29} and ν_{33} have strong contribution of C$_\alpha$−C$_\beta$ character, while ν_{35} mostly changes within the C$_\alpha$−C$_m$−C$_\alpha$ bond angle (slight negative correlation). As in A_{2g}, the linear modes within B_{2g} are classical skeletal modes with all changes occurring along the periphery of the ring.

Several infrared active modes of symmetry E_u (ip) (Figure S-ip of the Supporting Information) and A_{2u} (oop) (Figure S-oop of the Supporting Information) were found to have noticeable

Analysis of Core Size Effect in Metalloporphyrins

J. Phys. Chem. A, Vol. 112, No. 50, 2008 **12787**

sensitivity with respect to core size. Among them are degenerate E_u modes labeled as ν_{37}, ν_{38}, ν_{39}, ν_{41}, ν_{44}, ν_{46}, and ν_{49} and oop γ_9 modes (Figure 5, bottom). The E_u modes most sensitive to core size are ν_{37}, ν_{38} and ν_{39}, which have strong contributions from $C_\beta-C_\beta$ and $C_\alpha-C_m$ stretching, which increase and decrease, respectively, with core size for ν_{37} and follow the opposite trend for ν_{38}. Mode ν_{39} shows a decrease in the percent of $C_\beta-C_\beta$ stretching but a steady ($\sim$19%) contribution from $C_\alpha-C_m$. Symmetry block A_{2u} comprises significant oop modes γ_9, which are described as doming and inverted-doming vibrations.

The ip modes with high sensitivity to core size are mostly skeletal in nature; however, two exceptions exist. Modes ν_{18} (B_{1g}) and ν_{53} (E_u) have large slopes here-to-fore used as an indicator of core size sensitivity. However, there is no linear correlation of frequencies with increasing core size for these two modes. It is interesting to note that both are characterized by their large M−N contributions to total energy and that the graphical distribution of frequencies according to core size bear striking similarities among the metals with respect to the two modes (see the Supporting Information). All points lie in a similar pattern, and both Zn and Cr ($\sim$2.05 Å) lie far below and above the line of linearity, respectively, for each mode. The angle of the slope is slightly steeper for ν_{53}, but the change in frequency for all metals follows the same pattern for both modes. The M−N total energy for both modes is nearly identical for all metals with Fe only slightly higher for ν_{18}.

4. Summary and Conclusions

MPs are found in the active site of many proteins; therefore, research linking the structure and spectra of MPs has critical implications in a wide area of studies. Herein, we applied DFT to several unsubstituted planar MPs to elucidate how geometry and frequencies correlate with the M−N distance. Different transition metals can invoke expansion or contraction of the porphyrin core due to electronic effects resulting from the amount of d-electron pairing as well as occupancy of the $d_{x^2-y^2}$ orbital. The MnP has the largest core size with five unpaired electrons, and a domed porphyrin structure results when the Mn is pushed slightly out of plane. The smallest core size was found for NiP, with eight paired electrons, resulting in a distortion of the molecule and causing a ruffling of the planar structure. The computed range of M−N values (i.e., 1.96−2.09 Å) covers essentially the range of experimentally observed values. Peripheral substituents and effects associated with nonplanarity were not taken into account in the present study. For planar MPs, an analysis of geometry yielded a linear positive correlation for all skeletal bond lengths $C_\alpha-C_m$, $C_\beta-C_\beta$, and $C_\beta-C_\alpha$ and negative correlations for nitrogen-containing elements N−C_α. Changes in bond angles were more difficult to characterize, but the most notable were the $C_\alpha-C_m-C_\alpha$ and $C_\alpha-N-C_\alpha$ bends, which give credence to the suggestion by Warshel[20] that the methine bridges relieve strain caused by expansion of the core. Indeed, present DFT calculations confirm that the pyrrole rings can be viewed as rigid units with changes most notable for the $C_\alpha-N-C_\alpha$ angle. This prediction is consistent with normal coordinate deformation concept of Shelnutt, Jentzen, and co-workers.[23] They showed for out-of-plane distortions that all porphyrin deformations can be described as a linear combination of deformations along normal coordinates and that the coordinates of the lowest wavenumber modes are the dominant contributors to the deformation assignable to a distinct D_{4h} symmetry (a more formal argument can be found in ref 24). The core size changed considered in the

present study can be described as an A_{1g} type deformation. A check of the available normal modes of this symmetry type reveals that the corresponding lowest frequency mode (ν_9) involves changes of M−N, $C_\alpha-C_m$, and in-phase motion of the entire pyrrole rings.

A full vibrational analysis consisting of all 105 in-plane and out-of-plane frequencies was carried out, and the resulting modes were plotted against core size for a linear analysis and grouped within symmetry blocks. The modes were separated according to planarity, and all modes with a large slope and best fit greater than 0.8 were considered sensitive to M−N distance. All planar skeletal modes above 1450 cm^{-1} (ν_2, ν_3, ν_{10}, ν_{11}, ν_{19}, ν_{28}, ν_{37}, ν_{38}, and ν_{39}), as well as those with the majority of resultant vibrations from stretches or bends involving the core N (ν_{35}, ν_{49}, ν_{41}, ν_{25}, and ν_4), changed with the core as noted in the literature. The most significant out-of-plane modes sensitive to core size are γ_8 and γ_9, which are infrared-active and grouped within the A_{2u} symmetry block. By defining core-sensitive modes of MPs through a full vibrational analysis, it is then possible to establish correlation between frequencies and geometry. The linear dependence of certain frequencies allows for inverse correlation, that is, determination of structural changes in the porphine core from observed frequencies. Furthermore, analysis of the TED based on the natural internal coordinates indicates the structural element (bend, stretch, torsion, etc.) responsible for the specific vibration that links modes with linear dependence on core change. Overall, this work brings correlation of frequencies and structural properties to higher levels of accuracy and relativity as evident in the quality of the linear fit of frequencies to changes associated with the core expansion. The present work opens possible quantitative applications for the correlation of spectroscopic properties of MPs and heme proteins with actual structural parameters.

References and Notes

(1) (a) Dolphin, D., Ed. *The Porphyrins*; Academic: New York, 1978; Vols. *I−VI*. (b) Kadish, K. M., Smith, K. M., Guilard, R., Eds. *The Porphyrin Handbook*; Academic Press: San Diego, 2000. (c) Ortiz de Montellano, P. R., Ed. *Cytochrome P450: Structure, Mechanisms and Biochemistry*, 2nd ed.; Plenum Press: New York, 1995. (d) Dunford, H. B. *Heme Peroxidases*; Wiley-VCH: New York, 1999. (e) Scheer, H., Ed. *Chlorophylls*; CRC Press: Boca Raton, FL, 1991.

(2) See, for example, Spiro, T. G. *Biological Application of Raman Spectroscopy*; Wiley: New York, 1988; Vol *III*.

(3) Gouterman, M. *J. Mol. Spectrosc.* **1961**, *6*, 138–163.

(4) Spiro, T. G.; Strekas, T. C. *J. Am. Chem. Soc.* **1974**, *96*, 338–345.

(5) Hoard, J. L. *Science* **1971**, *174*, 1295–1302.

(6) Kitagawa, T.; Abe, M.; Kyogoku, Y. *J. Chem. Phys.* **1978**, *69*, 4526–4534.

(7) Spaulding, L. D.; Chang, C. C.; Yu, N.-T.; Felton, R. H. *J. Am. Chem. Soc.* **1975**, *97*, 2517–2525.

(8) Choi, S.; Spiro, T. G.; Langry, K. C.; Smith, K. M.; Budd, D. L.; La Mar, G. N. *J. Am. Chem. Soc.* **1982**, *104*, 4345–4351.

(9) Parthasarathi, N.; Hansen, C.; Yamaguchi, S.; Spiro, T. G. *J. Am. Chem. Soc.* **1987**, *109*, 3865–3871.

(10) Prendergast, K.; Spiro, T. G. *J. Am. Chem. Soc.* **1992**, *114*, 3793–3801.

(11) Frisch, M. J. Gaussian 03, Revision C.02; Gaussian, Inc.: Wallingford, CT, 2004; for the full reference, see the Supporting Information.

(12) Kozlowski, P. M.; Spiro, T. G.; Berces, A.; Zgierski, M. Z. *J. Phys. Chem. B* **1998**, *102*, 2603–2608.

(13) Kozlowski, P. M.; Rush, T. S., III; Jarzecki, A. A.; Zgierski, M. Z.; Chase, B.; Piffat, C.; Ye, B.-H.; Li, X.-Y.; Pulay, P.; Spiro, T. G. *J. Phys. Chem. A* **1999**, *103*, 1357–1366.

(14) Rush, T. S.; Kozlowski, P. M.; Piffat, C. A.; Kumble, R.; Zgierski, M. Z.; Spiro, T. G. *J. Phys. Chem. B* **2000**, *104*, 5020–5034.

(15) Stoll, L. K.; Zgierski, M. Z.; Kozlowski, P. M. *J. Phys. Chem. A* **2003**, *107*, 4165–4171.

(16) Yoshizawa, K.; Nakayama, T.; Kamachi, T.; Kozlowski, P. M. *J. Phys. Chem. A* **2007**, *111*, 852–857.

(17) (a) Pulay, P.; Fogarasi, G.; Pang, F.; Boggs, J. E. *J. Am. Chem. Soc.* **1979**, *101*, 2550. (b) Pulay, P.; Fogarasi, G. *J. Chem. Phys.* **1992**, *96*, 2856. (c) Fogarasi, G.; Zhou, X.; Taylor, P.; Pulay, P. *J. Am. Chem. Soc.* **1992**, *114*, 8191.

(18) Pulay, P.; Fogarasi, G.; Pongor, G.; Boggs, J. E.; Vargha, A. *J. Am. Chem. Soc.* **1983**, *105*, 7037–7047.

(19) Diebold, T.; Chevrier, B.; Weiss, R. *Inorg. Chem.* **1979**, *18*, 1193–200.

(20) Warshel, A. *Annu. Rev. Biophys. Bioeng.* **1977**, *6*, 273–300.

(21) Sparks, L. D.; Anderson, K. K.; Medforth, C. J.; Smith, K. M.; Shelnutt, J. A. *Inorg. Chem.* **1994**, *33*, 2297–2302.

(22) (a) Li, X. Y.; Czernuszewicz, R. S.; Kincaid, J. R.; Su, Y. O.; Spiro, T. G. *J. Phys. Chem.* **1990**, *94*, 31–47. (b) Li, X. Y.; Czernuszewicz, R. S.; Kincaid, J. R.; Stein, P.; Spiro, T. G. *J. Phys. Chem.* **1990**, *94*, 47–61.

(23) Jentzen, W.; Song, X.-Z.; Shelnutt, J. A. *J. Phys. Chem.* **1997**, *101*, 1684–1699.

(24) Schweitzer-Stenner, R.; Stichternath, A.; Dreybrodt, W.; Jentzen, W.; Shelnutt, J. A.; Nielsen, O. F.; Medforth, C. J.; Smith, K. M. *J. Chem. Phys.* **1997**, *107*, 1794–1815.